JACS
JOURNAL OF THE AMERICAN CHEMICAL SOCIETY

Article

pubs.acs.org/JACS

Structure Sensitivity of the Oxygen Evolution Reaction Catalyzed by Cobalt(II,III) Oxide

Craig P. Plaisance*,† and Rutger A. van Santen*

Institute for Complex Molecular Systems and Laboratory of Inorganic Materials Chemistry, Schuit Institute of Catalysis, Eindhoven University of Technology, 5612 AZ, Eindhoven, The Netherlands

Supporting Information

ABSTRACT: Quantum chemical calculations and simulated kinetics were used to examine the structure sensitivity of the oxygen evolution reaction on several surface terminations of Co_3O_4. Active sites consisting of two adjacent Co(IV) cations connected by bridging oxos were identified on both the (001) and (311) surfaces. Formation of the O−O bond proceeds on these sites by nucleophilic attack of water on a bridging oxo. It was found that the relative turnover frequencies for the different sites are highly dependent on the overpotential, with the dual-Co site on the (311) surface being most active at medium overpotentials (0.46−0.77 V), where O−O bond formation by water addition is rate limiting. A similar dual-Co site on the (001) surface is most active at low overpotentials (<0.46 V), where O_2 release is rate limiting, and a single-Co site on the (110) surface is most active at overpotentials that are high enough (>0.77 V) to form a significant concentration of highly reactive terminal Co(V)═O species. Two overpotential-dependent Sabatier relationships were identified based on the Brønsted basicity and redox potential of the active site, explaining the change in the active site with overpotential. The (311) dual-Co site that is most active in the medium overpotential range is consistent with recent experimental observations suggesting that a defect site is responsible for the observed oxygen evolution activity and that a modest concentration of superoxo intermediates is present on the surface. Importantly, we find that it is essential to consider the kinetics of the water addition and O_2 release steps rather than only the thermodynamics.

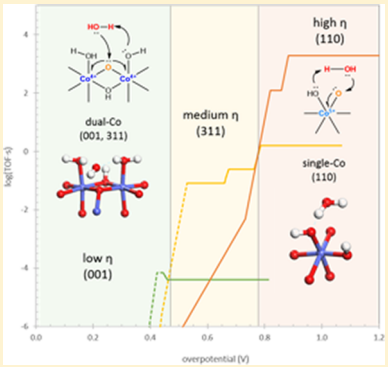

INTRODUCTION

While structure sensitivity of electrochemical reactions is well documented for transition-metal surfaces,[1−11] it has been investigated significantly less for reducible metal oxides. These oxides, particularly of the 3d transition metals, are promising and cost-effective catalysts for the oxygen evolution reaction (OER),[12−16] the reaction making the largest contribution to the overpotential in the electrolysis of water.[17,18] It is therefore of great importance to understand the mechanism of the OER on these materials, particularly with relation to the surface structure.

It is already known that surface structure can have a pronounced effect on the reactivity of transition-metal oxides in nonelectrochemical oxidation reactions.[19−24] Recently, Frei and co-workers have also discovered that the OER exhibits structure sensitivity on Co_3O_4 nanoparticles.[13,25,26] They find that <1% of the exposed Co cations account for most of the observed OER activity and propose the existence of an active site consisting of two electronically coupled Co cations. They additionally find a 16-fold increase in turnover frequency (TOF) for a bundled nanorod catalyst compared to a micron-sized particle, indicating that more of these active sites are present on the smaller particles. These results indicate that a defect site may be responsible for the OER activity. It should be noted that Co_3O_4 shares a structural motif, a Co_4O_4 cubane unit composed of octahedrally coordinated Co(III) cations, with the highly active CoPi OER catalyst developed by Nocera and co-workers.[12,27−29]

Here we present a computational study of the structure sensitivity of the OER on Co_3O_4 in order to identify the catalytic site that accounts for the experimentally observed activity. Computational investigation of the OER catalyzed by reducible metal oxides is an active field of study.[30−32] Different methods can be used to deduce the activity and overpotential of the reaction for a particular surface. A widely used approach, initiated by Rossmeisl, Nørskov, and others, is based on the thermodynamics of surface reaction intermediates only.[31,33] While pragmatic and useful for initial screening, this approach has a severe limitation (as has also been indicated by others)[34,35] that no reaction barriers are considered, and hence no prediction can be made of TOFs. We will show here that for Co_3O_4, a kinetic approach including reaction barriers is essential to correctly deduce the differences in reactivity of different sites.

The mechanistic choice of reaction in most previous studies is the decomposition of H_2O on a single surface cation to yield a terminal oxo ligand which then undergoes subsequent reactions to generate O_2.[36−38] We will discuss surface models where it appears that a dual-Co site containing reactive bridging

Received: July 24, 2015
Published: October 19, 2015

DOI: 10.1021/jacs.5b07779
J. Am. Chem. Soc. 2015, 137, 14660−14672

oxo ligands may have a higher reactivity under certain conditions. An important result is that the preferred site and mechanism depend on the applied potential.

The OER on both single-Co and dual-Co sites is studied on the (001) surface, which is the most energetically stable and extensively studied termination.[36] Additionally, we will discuss two other surfaces, the (110) and (311), that our studies show are more active than the (001) surface. The single-Co site is found to be faster on the (110) surface than on the (001) surface, and the dual-Co site is found to be faster on the (311) surface. As we will see, the enhanced activity on these two surfaces is due to differences in the local coordination environment of the active site. Our results on the (311) dual-Co site are in agreement with the experimentally determined overpotential, TOF, and reaction intermediates determined by Frei and co-workers,[13,25] suggesting that this is the highly active site observed in their study.

THEORETICAL METHODS

Computational Details. Quantum chemical calculations in this work are carried out using spin-polarized density functional theory (DFT) in the generalized gradient approximation (GGA), the details of which are given in the Supporting Information. A particular issue in applying this method to the study of 3d transition-metal oxides is an overdelocalization of the 3d electrons due to the presence of electron self-interaction in all such functionals.[39] An effective and low-cost method to correct for this is to apply an on-site self-interaction correction to the 3d electrons.[40−42] In this method, called GGA+U, the effective Coulombic repulsion integral between the 3d electrons (U) must be specified. For this work, we have determined a new value of U using a first-principles method adapted from the work of Cococcioni and de Gironcoli.[43,44] Further details are given in the Supporting Information.

Reaction Mechanism for the OER. We propose that the OER occurs in the following four steps which, similar to the mechanism proposed by Rossmeisl, Nørskov, and co-workers,[31] proceed through the formation of an intermediate hydroperoxo. Schematically, the reaction mechanism can be summarized in the following four steps. The first and third steps are composed of several quasi-equilibrated elementary steps that have been lumped together while the second and fourth steps are kinetically relevant elementary steps.

(1) $H_2O \rightleftharpoons O^{2-} + 2\,H^+$

(2) $O^{2-} + H_2O \rightleftharpoons HOO^- + H^+ + 2\,e^-$

(3) $HOO^- \rightleftharpoons O_2^- + H^+ + e^-$

(4) $O_2^- \longrightarrow O_2 + e^-$

In the first lumped step, the overall reaction is the dissociation of a water molecule over a vacancy on the active site, losing two protons and forming an oxo. The oxo then undergoes nucleophilic addition by a second water to form a hydroperoxo while releasing a proton and two electrons. In the third lumped step, the overall reaction is the oxidation of the hydroperoxo to a superoxo by release of an additional proton and electron. Finally, the superoxo loses an electron and desorbs as molecular oxygen, creating the vacancy onto which the first water dissociates. The mechanism is similar to one used in a previous theoretical study of the OER on Co_4O_4 clusters.[38]

At this point, we keep the mechanism general and do not specify where the protons and electrons are released to. The protons could be released to either the bulk electrolyte or to a basic site on the surface, while the electrons could be released to either the bulk electrode or to a hole localized at the surface. As already mentioned, the first and third steps are not necessarily elementary steps, and one or both of them are found to occur in multiple steps on all active sites studied. The elementary steps comprising these two composite steps, however, are not common to all active sites so they are not discussed at this point. They are analyzed in detail in the Results section.

The second and fourth steps, water addition and O_2 release, are nonelectrochemical so that the protons and electrons released in these steps are transferred to sites on the surface rather than the bulk electrolyte (protons) and the bulk electrode (electrons). This is supported by the experimental observations that the transfer coefficient is an integer and the current density is independent of changes in pH at constant overpotential, indicating that the rate-limiting step is nonelectrochemical.[27]

Unlike the second and fourth steps in the proposed mechanism which involve more complex chemical transformations, the first and third steps involve only proton and electron transfer. Experimental results showing zero-order dependence of the current density on the proton acceptor (HPO_4^{2-}) concentration in the electrolyte indicate that the rate-limiting step does not involve proton transfer to the electrolyte.[27] This is further supported by theoretical results showing activation barriers for proton transfer that are <0.1 eV higher than the reaction free energy.[45] Based on this evidence and the previously mentioned evidence that the rate-determining step is nonelectrochemical, we may assume that proton and electron transfers are fast compared to more complex chemical transformations so that the first and third steps are quasi-equilibrated.

Finally, we consider that proton and electron transfer to the bulk electrolyte and electrode are coupled so that chemical potentials of the proton and electron do not need to be specified separately. As a result, we only need to consider neutral surfaces in our calculations. This assumption is supported by the already mentioned experimental observation that the current density is independent of pH at constant overpotential.[27]

We neglect the effect of the electrolyte on the thermodynamics and kinetics of surface processes as is also done in other theoretical studies of the OER on oxide surfaces.[30,31,36,46] This has been justified by a theoretical study showing that the interactions between solvent water molecules and the adsorbates are <0.05 eV.[31] Although our model does not include the electrolyte, it does allow for strongly adsorbed and dissociated water in the first layer and the interaction of an additional water molecule with the transition state on the (110) site, both of which are discussed in more detail in the Supporting Information.

There is one other mechanism often proposed in the literature that involves the direct radical coupling between two adjacent η-oxo ligands to form an η^2-peroxo.[38,47] While some computational studies support this mechanism,[48,49] other studies,[36,38] including ours, suggest that the energy required to form two η-oxos is too high for this mechanism to be feasible. Since, as we show later, the energy to form even one η-oxo is high, it is likely that this mechanism is only feasible at very high overpotentials. We discuss the possibility of this mechanism in more detail later.

Kinetic Simulation. As discussed in the previous section, in our model either water addition or O_2 release is rate limiting. As shown in the Supporting Information, for an irreversible serial catalytic cycle with two kinetically relevant steps, the TOF at steady state can be written:

$$\mathrm{TOF} = \frac{1}{\frac{1}{\mathrm{TOF}_1} + \frac{1}{\mathrm{TOF}_2}} \tag{1}$$

where TOF_1 (TOF_2) is the TOF if the first (second) step is rate limiting. It can be seen from the expression that the actual rate-limiting step will be the one with the lowest TOF since this term will be larger in the denominator.

To determine the quantities TOF_n in eq 1, we first note that at a given overpotential there is an equilibrium distribution between all of the possible resting states of the surface that are connected by processes other than reaction n. The probability to find the surface in a particular resting state j is given by the Boltzmann distribution considering all possible resting states i of the active site, including state j:

DOI: 10.1021/jacs.5b07779
J. Am. Chem. Soc. 2015, 137, 14660−14672

$$\theta_j = \left[\sum_i \exp\left(\frac{\Delta G_{ij} - e\eta\Delta n_{ij}}{k_B T}\right)\right]^{-1} \quad (2)$$

The term ΔG_{ij} is the free energy difference between resting states j and i at an overpotential of zero (1.23 V vs SHE) and is computed according to the method of Nørskov, Rossmeisl, and co-workers[31,33] as detailed in the Supporting Information. At overpotentials different from zero, this energy changes by an amount equal to the overpotential η multiplied by the quantity Δn_{ij}, the number of oxidations (removal of one proton and one electron) required to get to resting state j from resting state i. At most overpotentials, one term in the sum in eq 2 will be much larger than the others so that the others can be neglected. This state, the one with the lowest free energy, is the dominant resting state. At an overpotential of zero, it is typically the surface in which all Co cations in the surface layer are in their bulk oxidation state (Co(III) for those in octahedral sites) and are fully coordinated by water and hydroxo ligands. As the overpotential increases, surfaces in which Co(III) cations are oxidized to Co(IV) (coupled with deprotonation of water and hydroxo ligands) become more stable relative to the reduced surface. As a result, the degree of oxidation of the dominant resting state increases. This is discussed for the different surfaces in detail in the Supporting Information.

In determining TOF_n, reaction n can proceed from any of the possible resting states j containing the appropriate reactive intermediate, not just the dominant resting state. This TOF therefore includes the contributions from all of these resting states:

$$TOF_n = \frac{k_B T}{h} \sum_j \exp\left(-\frac{\Delta G_j^{\ddagger}}{k_B T}\right)\theta_j \quad (3)$$

where $\Delta G_j^{\ddagger}$ is the free energy difference between a transition state and the resting state j preceding it, while θ_j is the probability that the active site is in a resting state j, given by eq 2.

As with eq 2, one term in the sum in eq 3 will typically be much larger than the others, and the TOF can be approximated by a single term which corresponds to the dominant transition state. When this is the case, the TOF can be written in terms of only the dominant transition state j (proceeding from resting state j) and the dominant resting state i:

$$TOF_n = \frac{k_B T}{h} \exp\left(-\frac{\Delta G_j^{\ddagger} + \Delta G_{ij} - e\eta\alpha_{ij}}{k_B T}\right) \quad (4)$$

The parameter α_{ij}, called the transfer coefficient, is equal to Δn_{ij}, the number of oxidations required to go from the dominant resting state i to the resting state j preceding the dominant transition state. As will be seen in the Results section, this parameter determines the way in which the TOF increases with overpotential and is related to the experimentally measured Tafel slope β by $\alpha = k_B T/e\beta$, where e is the elementary electric charge.

For the OER at a single-Co site on both the (001) and (110) surfaces, we have found that the water addition step is rate limiting under all conditions examined, in agreement with an aforementioned study on Co_4O_4 clusters.[38] At a dual-Co site, the rate-limiting step is found to depend on the overpotential. At lower overpotentials, the equilibrium concentration of the superoxo is significantly less than the concentration of the oxo so that O_2 release is rate limiting. As the overpotential increases, the concentration of superoxo increases relative to the oxo so that water addition becomes rate limiting instead.

RESULTS

We first present the elementary steps and intermediates involved in the catalytic cycles on the single-Co site on the (110) surface and the dual-Co site on the (311) surface along with the energetics of these steps. Both sites carry out O−O bond formation by initial oxidation of the Co cation(s) to an active state which then undergoes nucleophilic addition of water to an oxo ligand. For the dual-Co site, it is found that the initial oxidation occurs at a lower overpotential, but the subsequent water addition has a higher intrinsic activation barrier compared to the single-Co site. A quantum chemical analysis of the water addition reaction is then presented which rationalizes the difference in energetics between the two sites. Finally, the results of the kinetic model at different overpotentials are presented. This shows that even though the intrinsic barrier for water addition at the single-Co site is lower, the dual-Co site has a higher TOF at low overpotentials due to the lower overpotential required for oxidation of the two cobalt centers to Co(IV) compared to oxidation of the single-Co site to Co(V). At high overpotentials, the greater reactivity of the terminal oxo on the single-Co site prevails.

Catalytic Cycles on the Different Surfaces. *Single-Co Site.* In most previous studies,[36−38] it has been assumed that O−O bond formation occurs through the addition of water to an η-oxo bound to a single Co cation. We find that this process occurs on the (110) surface by the catalytic cycle shown in Scheme 1 at overpotentials between 0.82 and 0.86 V. Similar catalytic cycles operate at other overpotentials, although the energetics are slightly different. The η-oxo, initially coordinated to Co(V), first undergoes nucleophilic attack by a solvent water molecule. During this step, the water transfers a proton to an adjacent η-OH and then forms an O−O bond with the oxo leading to an η-OOH. In this process, which has an activation barrier of 0.63 eV, two electrons are transferred from the two reacting oxygen atoms to the Co(V), reducing it to Co(III). In the next step, the hydroperoxo is oxidized electrochemically to a superoxo by loss of an electron and proton. The superoxo is unstable and spontaneously loses an electron to a hole on a nearby subsurface Co(IV) (indicated by e^- in the schematic), subsequently desorbing as O_2 and being replaced by a second molecule of water. In the same step, the water molecule that just adsorbed transfers a proton to an η-OH on a nearby site, coupled with the transfer of an electron from the Co(III) in the active site to a hole on another nearby subsurface Co(IV) (indicated in the schematic by H^+ and e^-, respectively). The oxidation and subsequent O_2 release (and replacement by water) is very exoergic and has a reaction free energy of −1.82 eV at zero overpotential. Furthermore, there is no non-electrochemical activation barrier for O_2 release since the superoxo is unstable. Following O_2 release, the cobalt at the active site is reoxidized to Co(V), and the nearby subsurface Co cations (not shown in the schematic) are reoxidized to Co(IV) in three sequential electrochemical steps (coupled with the loss of three protons) to complete the catalytic cycle. Formation of the Co(V) is difficult and has an oxidation overpotential of 0.80 V. This mechanism is similar to one proposed by Siegbahn and co-workers for a Co_4O_4 cubane cluster,[38] although the order of some of the steps is different. A similar catalytic cycle is found for the single-Co site on the (001) surface, depicted in the Supporting Information.

Dual-Co Site. We additionally find that O−O bond formation can occur by water addition to a μ^3-oxo on a dual-Co site in the catalytic cycle shown in Scheme 1 for the (311) surface. This cycle starts with a μ^3-O coordinated to two Co(IV) cations (and one Co(II) that is not shown). The oxo undergoes nucleophilic attack by a solvent water molecule which first transfers a proton to a neighboring η-OH before forming an O−O bond with the μ^3-O, leading to a μ^3-OOH.

Instead of transferring two electrons to a single Co(V), as was the case for the single-Co site, each of the two electrons is

DOI: 10.1021/jacs.5b07779
J. Am. Chem. Soc. 2015, 137, 14660−14672

Scheme 1. Catalytic Cycles and Energetics (eV at η = 0) of the OER for the Single-Co Site on the (110) Surface and the Dual-Co Site on the (311) Surface[a]

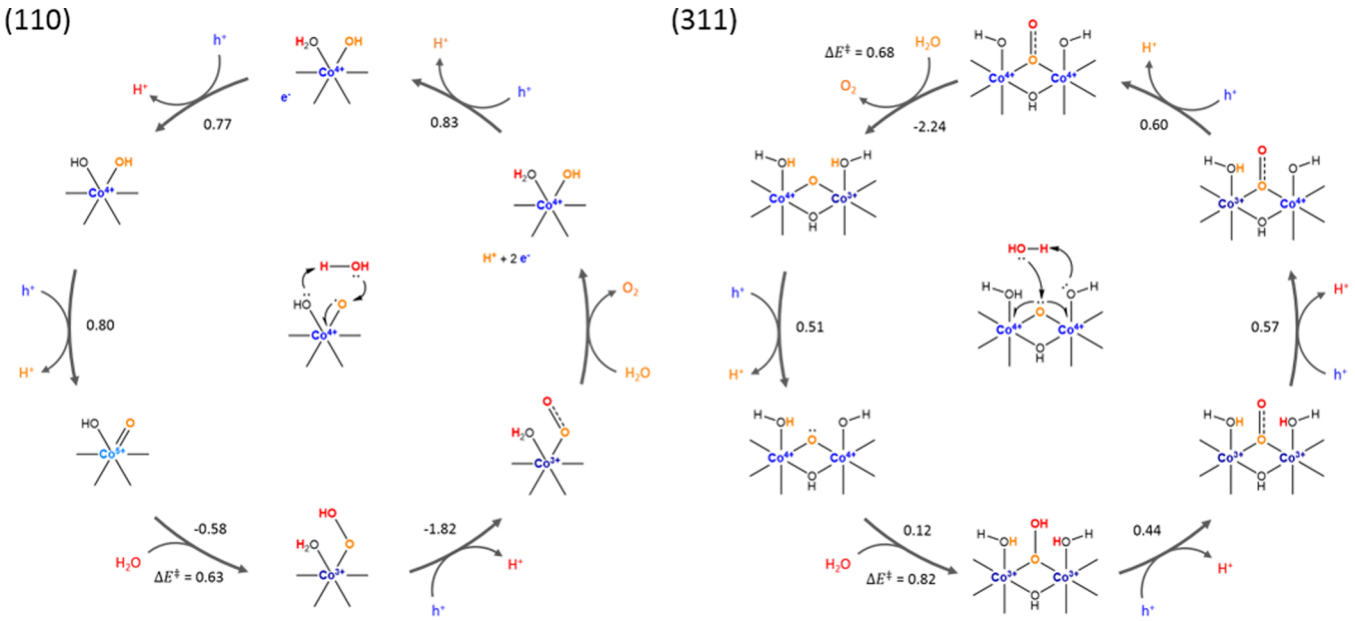

[a]H^+ and e^- labels in the structures indicate protons and electrons located at a nearby site that is not shown in the structure. The particular cycle shown for the (110) site operates at overpotentials between 0.82 and 0.86 V, while the cycle shown for the (311) site operates at overpotentials between 0.51 and 0.66 V.

transferred to one of the two Co(IV) cations adjacent to the bridging oxo, reducing them to Co(III). This step has an activation barrier of 0.82 eV, higher than on the (110) single-Co site. Distribution of the two holes needed to oxidize the incoming water in the O−O bond forming step on two Co(IV) centers rather than one Co(V) center lowers the free energy to oxidize the active site prior to water addition from 0.80 to 0.51 V but increases the intrinsic activation barrier of water addition from 0.63 to 0.82 eV.

Following O−O bond formation, the hydroperoxo is oxidized electrochemically to a superoxo followed by the electrochemical oxidation of both of the Co(III) cations in the active site to Co(IV). Each of these three oxidations is accompanied by the release of a proton. The superoxo then transfers an electron to one of the Co(IV) and desorbs as molecular oxygen, being replaced by a dissociated water.

Unlike the single-Co site, the O_2 release step on the dual-Co site is activated since the electron transfer does not occur until after the O_2 is partially desorbed. It is, however, still a very exoergic step with a decrease in free energy of 2.24 eV. Finally, the resulting Co(III) is oxidized electrochemically to Co(IV) along with the loss of a proton from a water ligand (with an oxidation overpotential of 0.51 V), restarting the catalytic cycle. A similar cycle, presented in the Supporting Information, operates on the dual-Co site on the (001) surface.

The participation of two Co(IV) cations rather than a single Co(V) cation in the water addition step is similar to the mechanism proposed by Frei and co-workers,[25] also involving a dual-Co site. However, in our mechanism, water adds to a bridging oxo, while they suggest water adds to a terminal oxo bound to one of the Co(IV) cations. The presence of Co(IV) in the working catalyst has been confirmed by electron paramagnetic resonance[50] and X-ray absorption spectroscopy.[29]

In the next section, we examine the electronic transitions that occur during the water addition reaction that are responsible for the differences in this step between the dual- and single-Co sites.

Quantum Chemical Considerations on O−O Bond Formation Steps. The higher intrinsic reactivity for water nucleophilic addition to an η-oxo on a single-Co site compared to a μ^3-oxo on a dual-Co site can be understood by examining this reaction at the quantum chemical level on the two sites. On both sites, water addition is found to proceed by an initial proton-coupled electron transfer (PCET) followed by formation of the O−O bond in the hydroperoxo product. On the single-Co site, O−O bond formation occurs concertedly with the PCET since, after the electron transfer, both holes required to oxidize the water reside on the oxo. On the dual-Co site, only a single hole is present on the oxo after the PCET, and an additional electron must be transferred from the oxo to the other Co(IV) before the O−O bond can form. The energetic cost of this additional redox process results in a much higher activation barrier. In the next two sections, the complex succession of changes in electronic structure in combination with the deprotonation of water that occurs during O−O bond formation on the two sites is discussed in more detail. A more detailed discussion is provided in the Supporting Information.

Single-Co Site. Water addition to a terminal oxo on the (110) single-Co site begins with the oxo bound to a Co(V) cation. During the course of the reaction, one electron is formally transferred from each of the oxygen atoms forming the O−O bond to the Co(V). In the initial state, the two holes needed to oxidize the two oxygen atoms are localized in a pair of π^* orbitals associated with the Co=O bond, with parallel spins (triplet state). The density distributions of the two holes are shown in the first structure of Scheme 2a. Despite the presence of two high energy holes in the π^* orbitals, this species is not reactive for water addition because the holes have the same spin, while formation of the O−O bond requires transfer of two electrons with opposite spin. This species first

DOI: 10.1021/jacs.5b07779
J. Am. Chem. Soc. 2015, 137, 14660−14672

Scheme 2. Mechanism of Water Addition to (a) a Terminal Oxo on a Single-Co Site and (b) a Bridging Oxo on a Dual-Co Site along with Density Distributions of the Holes (green = spin-up; blue = spin-down; grey = both spins) at Different Points along the Reaction Trajectory[a]

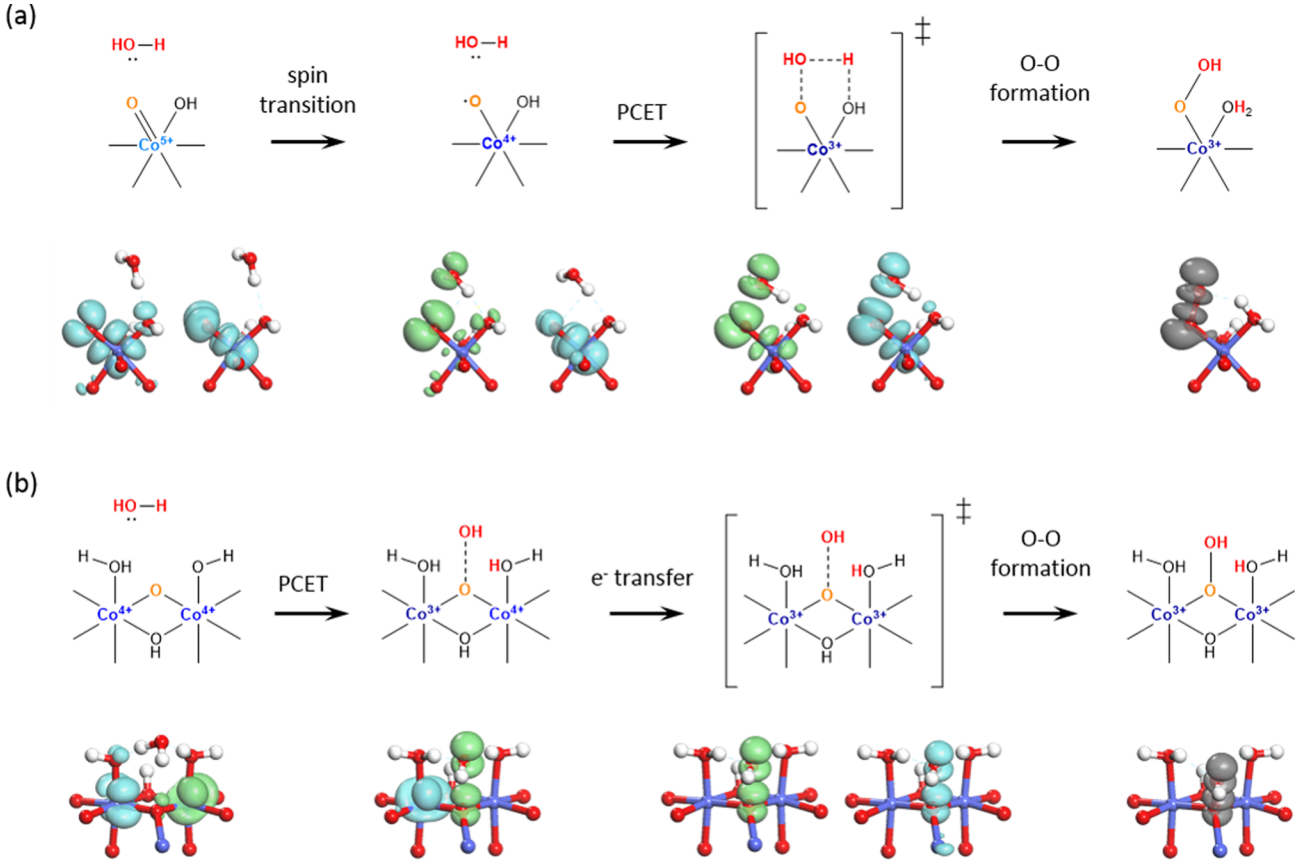

[a]The method for determining the hole-densities is discussed in the Supporting Information.

transitions to a singlet state that is 0.18 eV higher in energy than the triplet state. Due to spin polarization of the π and π^* orbitals containing the two holes, this configuration is best characterized as a Co(IV) with a single bond to an O^- radical so that one hole resides mainly in an oxygen 2p orbital and the other mainly in a Co 3d t_{2g} orbital (shown in the second structure of Scheme 2a).

Water addition to the singlet Co═O commences by transfer of a proton from the water to a hydroxo ligand that is also coordinated to the Co center. This proton transfer is not favorable when the Co is in the +IV oxidation state due to the low basicity of the hydroxo bound to an electrophilic Co(IV). As a result, an electronic transition occurs during the proton transfer in which an electron is transferred from a state centered on a 2p orbital on the oxo to an empty state centered on a 3d t_{2g} orbital on the Co(IV), reducing the latter to Co(III). At this point, both holes reside in states centered on a 2p orbital on the oxo and further enhance deprotonation of the attacking water by accepting the donation of negative charge from a lone pair on the resulting hydroxide (seen by delocalization of the hole onto the oxygen of the attacking water in the third structure of Scheme 2a). This leads to the formation of an O−O bond as the proton transfer continues, eventually forming the hydroperoxo in the product state with the holes residing in the O−O σ^* orbital (fourth structure of Scheme 2a).

The transition state for the water addition reaction coincides with the above-mentioned electronic transition during the PCET. This occurs at the point where the potential energy surfaces corresponding to the two electronic states cross (third structure of Scheme 2a). Due to the electronic transition that occurs at the transition state, conventional methods of locating it such as the nudged elastic band and the dimer method cannot be used, leading us to develop an alternative method for locating it that is described in the Supporting Information. The transition state that we identify is 0.45 eV above the singlet Co(IV)−O state and 0.63 eV above the triplet Co(V)═O state.

Water addition occurs by a similar pathway on the (001) single-Co site.

Dual-Co Site. Unlike the single-Co site in which the two holes that oxidize the attacking water initially reside on a single Co(V) center, these holes reside on separate Co(IV) centers in the (311) dual-Co site (first structure of Scheme 2b). Nevertheless, water addition to this site begins in a similar way as it did for the single-Co site, with the first step involving a PCET. In this step, the water transfers a proton to an η-hydroxo coordinating one of the Co(IV) centers of the active site, while an electron is transferred from a 2p orbital on the μ^3-oxo to an empty 3d t_{2g} orbital on the other Co(IV) center, reducing it to Co(III). In contrast to the two holes on the η-oxo of the single-Co site, the single hole centered on the μ^3-oxo of the dual-Co site is not sufficient for forming an O−O bond with the attacking water since one electron still resides in the σ^* orbital. As a result, the initial PCET leads to a high-energy

DOI: 10.1021/jacs.5b07779
J. Am. Chem. Soc. 2015, 137, 14660−14672

intermediate in which this hole is delocalized between the μ^3-oxo and the hydroxide formed from the deprotonated water (second structure of Scheme 2b). This intermediate has an energy 0.48 eV higher than the reactant state. Formation of the O−O bond requires a second electron transfer from the σ^* orbital to an empty 3d t_{2g} orbital on the remaining Co(IV) center, requiring an additional energy of 0.34 eV. The transition state corresponds with this second electron transfer and occurs at the crossing point of the potential energy surfaces for the two electronic states (third structure of Scheme 2b). This transition state has an energy 0.82 eV above the initial state where both Co centers were in the +IV oxidation state. After the second electron transfer, both holes reside in the O−O σ^* orbital (fourth structure of Scheme 2b).

Water addition occurs by a similar pathway on the (001) dual-Co site.

Summary of Quantum Chemical analysis. The above discussion shows that the much higher intrinsic activation barrier for water addition to the dual-Co site compared to the single-Co site arises from the additional redox energy associated with the transfer of a second electron from the μ^3-oxo to a Co(IV) to create the two holes on the μ^3-oxo required to form an O−O bond with the attacking water. This agrees with the finding that the energetics of the PCET processes are similar for the single-Co (110) and dual-Co (311) sites, estimated as the reduction potential for adding a proton and electron to the active site (−1.82 and −1.74 V, respectively, versus the standard hydrogen electrode), suggesting that this component of the water addition reaction is not responsible for the large difference in activation barriers.

Because of the strong Coulombic repulsion that would result from having both holes localized on a single Co center, one hole is already localized on the oxo in the initial singlet state of the single-Co site. Consequently, the two holes required to form the O−O bond are both centered on the oxo after the PCET on this site so that the O−O bond can form immediately afterward without the need for the additional electron transfer that was required on the dual-Co site.

TOF vs Overpotential. Figure 1 shows the TOF of the OER as a function of overpotential on the four different active sites on the (001), (110), and (311) surface terminations. The TOFs were calculated according to eq 4 where it is assumed that the kinetic expression is dominated by a single resting state and transition state. It is seen that the TOF increases as the overpotential increases, with several discontinuities in the slope. There are two mechanisms responsible for these behaviors. The first is related to the fact that the dominant transition state in eq 4 often proceeds from a resting state (the active resting state) that is more oxidized than the dominant resting state due to the fact that the intrinsic barriers for water addition and O_2 release are typically lower for more oxidized surfaces (discussed further in the Supporting Information). Consequently, an electrochemical pre-equilibrium exists between the dominant resting state and the active resting state. As the overpotential increases, the equilibrium shifts toward the more oxidized active resting state. This leads to an increase in the logarithm of the TOF with overpotential that is proportional to the transfer coefficient α, the number of oxidations associated with the pre-equilibrium. Since both of the kinetically relevant steps are nonelectrochemical, the transfer coefficient arises solely from the pre-equilibrium and is thus always an integer, in agreement with certain experimental results on Co-based OER catalysts.[27] The points in Figure 1 where the slope increases correspond to

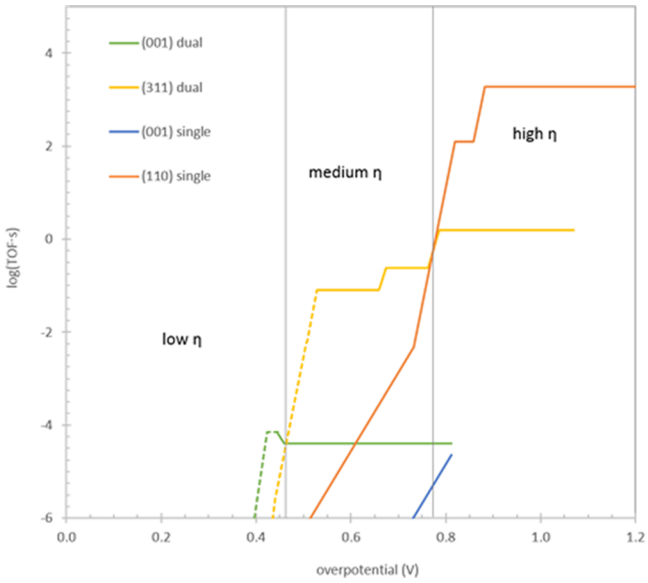

Figure 1. TOF of the OER on the dual-Co sites on the (001) and (311) surfaces and the single-Co sites on the (001) and (110) surfaces as a function of overpotential. The three overpotential regimes are indicated. Solid curves show the regions where H_2O addition is rate limiting. Dashed curves show the regions where O_2 release is rate limiting.

changes in the dominant transition state to one proceeding from a more oxidized active resting state so that the number of oxidations involved in the pre-equilibrium increases.

The second way in which increasing the overpotential affects the TOF is due to the progression of the dominant resting state to an increasingly more oxidized surface. At the overpotentials where this occurs, the slope in Figure 1 decreases due to a decrease in the number of oxidations involved in the pre-equilibrium. When the dominant transition state proceeds from an active resting state having the same degree of oxidation as the dominant resting state, the TOF no longer increases with overpotential. Such decreases in the transfer coefficient are observed in electrochemical measurements of the OER activity on several transition-metal oxides,[14] although this behavior could also be due to changes in the mechanism or rate-limiting step. The specific dominant resting and transition states at the different overpotentials on each site are shown in the Supporting Information. Once the surface is completely oxidized, the TOF ceases to increase with overpotential since increasing the overpotential will not oxidize the surface further, although in reality it may lead to a change in the bulk phase.

Only three of the four curves shown in Figure 1 are relevant for determining the overall activity of the catalyst; the single-Co site on the (001) surface is not dominant at any of the overpotentials examined. Furthermore, there are two points where the curves with the highest TOF cross, at 0.46 and 0.77 V, indicating that at these overpotentials there is a change in the active site. This leads to three different potential regimes: a low potential regime dominated by the dual-Co site on the (001) surface, a medium potential regime dominated by the dual-Co site on the (311) surface, and a high potential regime dominated by the single-Co site on the (110) surface. Interestingly, it is the middle regime that corresponds to the measurements made by Frei and co-workers ($\eta \approx 0.5$ V).[25] Our calculated TOF on the (311) surface at this overpotential is in

DOI: 10.1021/jacs.5b07779
J. Am. Chem. Soc. 2015, 137, 14660−14672

fairly good agreement with their results (~3 s^{-1}), while the TOFs on the other surfaces are much lower.

Figure 1 also shows for each active site the overpotentials where oxygen release is rate limiting. This occurs only on the dual-Co sites, at overpotentials below 0.45 V on the (001) surface and below 0.53 V on the (311). Oxygen release is never rate limiting on the single-Co sites over the range of overpotentials we have examined.

The overpotential of 0.5 V corresponding to the measurements of Frei and co-workers falls within the O_2 release-limited regime on the (311) dual-Co site. This is consistent with their observation of superoxide species on the surface, which is the precursor to O_2 release. The fact that only the (311) surface is limited by oxygen release at this overpotential, combined with the agreement with the experimentally measured TOF and the observed structure sensitivity, strongly indicates that this specific site on the (311) surface is the active site observed in the experiment.

DISCUSSION

As just seen, the results of our kinetic analysis indicate that the most active site for the OER varies according to the overpotential, leading to three overpotential regimes, each dominated by a different active site on a different surface termination. There are two boundaries separating the three potential regimes shown in Figure 1: the first occurring at an overpotential of 0.46 V where the dual-Co site on the (311) surface overtakes the dual-Co site on the (001) surface and the second occurring at an overpotential of 0.77 V where the single-Co site on the (110) surface overtakes the dual-Co site on the (311) surface. In the following discussion, we compare the way that the overpotential controls the TOFs on the different sites and elucidate the origin of the three potential regimes.

We will then compare our kinetics-based approach to the widely used thermodynamics-based approach of Rossmeisl, Nørskov, and co-workers,[31] where it will be seen that calculating activation barriers for water addition and O_2 release is essential for predicting the dominant active site at a given overpotential. Finally, we compare our results to the experimental results of Frei and co-workers pertaining to the OER on Co_3O_4 nanoparticles[25] and conclude that the very active site they observe is likely the dual-Co site on the (311) surface.

Kinetic Overpotential Regimes and Sabatier Relations. It will be seen in the following discussion that the two regime transitions observed in Figure 1 are related to two qualitative changes in the reaction kinetics. The transition between the low ((001) dual-Co site) and medium ((311) dual-Co site) potential regimes is related to a change in the rate-limiting step on the dual-Co sites from O_2 release to water addition, while the transition between the medium and high ((110) single-Co site) potential regimes is related to a change in the dominant resting state of the Co cation in the single-Co site on the (110) surface from Co(IV) to Co(V). In the following discussion, we will see that these two regime transitions are related to two potential-dependent Sabatier relationships that govern the TOF—one based on the Brønsted basicity of the oxygen atoms in the site and the other based on the oxidation potential. It thus appears that there is a two-parameter Sabatier relation, shown qualitatively in Scheme 3, governing the TOF of the OER on the different active sites. This relationship is discussed in more detail in the following sections.

Scheme 3. Schematic Depiction of the Sabatier Relationship Based on Oxygen Brønsted Basicity and Oxidation Potential of the Active Site[a]

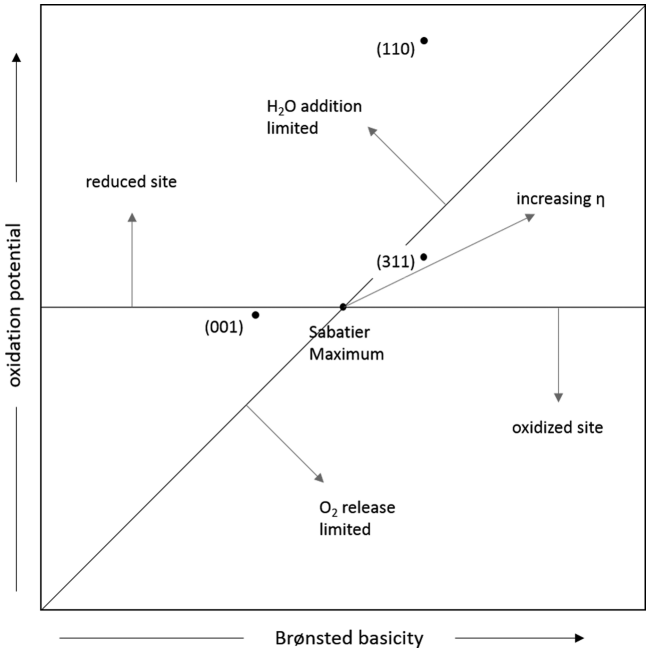

[a]The parameter space is divided into four quadrants by two lines: the horizontal line separates the sites that are oxidized in the resting state and those that are reduced. The diagonal line separates the sites that are limited by H_2O addition and those that are limited by O_2 release. The arrow labeled "increasing η" indicates that the Sabatier maximum moves to a site with higher basicity and oxidation potential as the overpotential is increased. The qualitative positions of the (001) and (311) dual-Co sites and the (110) single-Co site are indicated at an overpotential corresponding to the transition between the low and medium potential regimes.

Low–Medium Potential Regime Transition; Relation to Brønsted Basicity. At an overpotential of 0.46 V, a transition occurs between the low potential regime, where the (001) dual-Co site has the highest TOF, to the medium potential regime, where the (311) site has the highest TOF. This transition is associated with a change in the rate-limiting step on the dual-Co sites from O_2 release to water addition which occurs at 0.45 V on the (001) site and 0.53 V on the (311) site. O_2 release is faster on the (001) site than on the (311) site; therefore, in the low potential regime where O_2 release is rate limiting, the (001) site has a higher TOF. Conversely, water addition is faster on the (311) site so that this site has a higher TOF in the medium potential regime where water addition is rate limiting. In the following discussion, we will see that the differences in the rates of these two elementary steps on the two sites are related to the Brønsted basicity of the oxygen atoms in the active site.

Reason for Faster O_2 Release on the (001) Site. To rationalize the faster rate of O_2 release on the (001) site compared to the (311) site, we compare the energetics on the two sites, shown in Figure 2, at an overpotential of 0.40 V. This is the overpotential where the ratio between the rates of O_2 release on the (001) site compared to the (311) is maximum (2–3 orders of magnitude). To form O_2 from the dominant resting state at this potential, the site is first oxidized once on the (311) surface or twice on the (001) surface followed by water addition (in the dominant resting state for the (311)

DOI: 10.1021/jacs.5b07779
J. Am. Chem. Soc. 2015, 137, 14660–14672

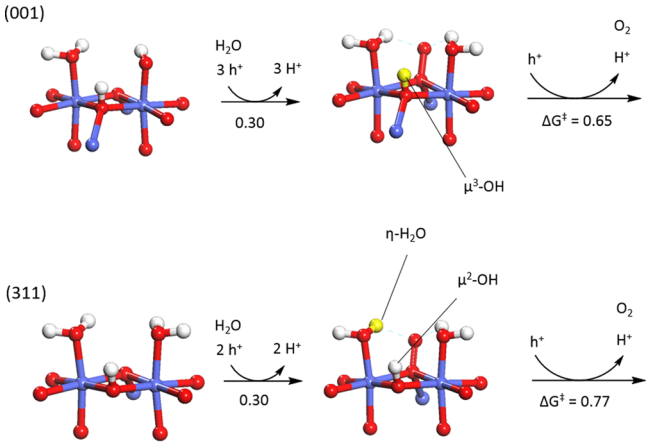

Figure 2. Comparison of the structures and energetics (eV at η = 0.4 V) of O_2 release by the dual-Co sites on the (001) and (311) surfaces. The first step combines oxidation of the active site, water addition, and oxidation of the hydroperoxo to a superoxo. The second step is the oxidation of the superoxo to O_2 and its release. The (001) site has a lower barrier for the second step because a more acidic μ^3-OH is deprotonated rather than the less acidic η-H_2O on the (311) site.

surface at this potential, the active site already has one of the two Co centers in the +IV oxidation state). The resulting hydroperoxo then loses a proton and electron to form a superoxo intermediate which then loses another proton and electron to release O_2. From Figure 2, we can see that at this overpotential the energy of the superoxo with respect to the resting state is exactly the same on the two sites, 0.30 eV. The higher apparent barrier for O_2 release on the (311) site (1.07 vs 0.94 eV) is therefore due to the energy required to oxidize the superoxo to dioxygen, which is higher on the (311) site by 0.12 eV.

Oxidation of the superoxo to dioxygen involves removal of an electron from an O−O π^* orbital and removal of a proton from the surface, hence it depends on the Brønsted acidity of the surface water and hydroxo ligands. On the (001) surface, the proton is removed from a μ^3-OH group, while on the (311) surface the proton is removed from an η-H_2O. The μ^3-OH is more acidic than the η-H_2O resulting in a lower energy for the oxidation step on the (001) site. On the (311) surface, the μ^3-OH is instead a μ^2-OH due to the location of the active site on a step edge, as shown in Figure 2. Due to the lower coordination of the μ^2-OH oxygen atom by Co cations, this species is less acidic than both the μ^3-OH and the η-H_2O (the order of acidity is μ^2-OH < η-H_2O < μ^3-OH) so that the η-H_2O is the species that deprotonates during this step.

Reason for Faster Water Addition on the (311) Site. The higher rate of water addition on the (311) dual-Co site compared to the (001) dual-Co site, which is responsible for the (311) site having the higher TOF in the medium potential regime, is due to a higher intrinsic activation barrier for this reaction on the (001) site. There are two properties of the active site that control this barrier: the electrophilicity and the oxygen Brønsted basicity. The electrophilicity is required for the oxo to accept the lone pair donated from the attacking water and is similar for both dual-Co sites so does not have a large influence on the difference in the activation barriers on these two sites. It will be seen later that the electrophilicity does play an important role in the transition between the medium and high potential regimes. The basicity is required to deprotonate the attacking water before it can form an O−O bond to the oxo and is the factor responsible for the higher barrier on the (001) site. On the (311) site, the proton is transferred to an η-OH, while on the (001) site, it is transferred to a less basic μ^3-O as shown in Figure 3. The η-OH is not

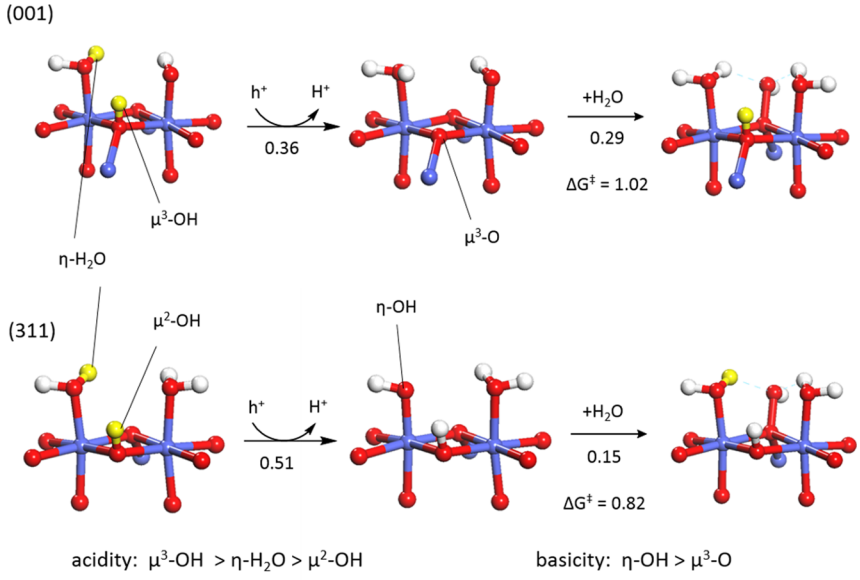

Figure 3. Comparison of the structures and energetics (eV at η = 0) of water addition to a dual-Co site on the (001) and (311) surfaces. The first step is the oxidation of the site by removal of an electron and proton, and the second step is deprotonation of the attacking water and formation of the hydroperoxo. On the (001) site, the μ^3-OH deprotonates in the first step forming a μ^3-O that deprotonates the water in the next step. On the (311) site, this OH is coordinated by only two Co cations due to the location of the site on a step edge. This μ^2-OH is less acidic than the η-H_2O, which deprotonates instead to form an η-OH. The η-OH on the (311) site is more basic than the μ^3-O on the (001) site and more easily deprotonates the attacking water, leading to a less endothermic water addition with a lower barrier.

DOI: 10.1021/jacs.5b07779
J. Am. Chem. Soc. 2015, 137, 14660−14672

formed on the (001) surface because the η-H_2O from which it is formed is less acidic than the nearby μ^3-OH, having a deprotonation energy that is 0.24 eV higher. Instead, this latter species deprotonates in the electrochemical oxidation step preceding water addition to form the μ^3-O.

Relation to Oxygen Brønsted Basicity. The μ^3-OH and η-H_2O which form the μ^3-O and η-OH that accept a proton during water addition are exactly the same sites that deprotonate during the oxidation of the superoxo to dioxygen. The more acidic μ^3-OH on the (001) site deprotonates more easily during O_2 release, while the less acidic η-H_2O on the (311) site has a stronger conjugate base that more easily deprotonates the water in the O−O bond formation step. This suggests a Sabatier principle relating O−O bond formation and O_2 release to the Brønsted basicity (or acidity) of the site as shown in Scheme 3; as the basicity increases (acidity decreases) O−O bond formation (involving protonation) becomes faster, while O_2 release (involving deprotonation) becomes slower. The region of the diagram to the top-left of the Sabatier maximum (low basicity) corresponds to rate limiting water addition where an increase in basicity leads to an increase in TOF. The region to the bottom-right of the Sabatier maximum (high basicity) corresponds to rate limiting O_2 release where an increase in basicity leads to a decrease in TOF. The line dividing the low and high basicity regions is not vertical but diagonal because an increase in oxidation potential correlates with a more exothermic water addition reaction which in turn leads to a greater superoxo concentration and faster O_2 release compared to water addition.

The Sabatier curve is not fixed, however, and changes position as the overpotential increases. This is due to the effect of overpotential on the relative rates of water addition and O_2 release. At most overpotentials, two oxidations must occur between water addition and O_2 release: oxidation of the hydroperoxo formed from water addition to a superoxo and oxidation of the superoxo to O_2. These oxidations are endoergic up to overpotentials of about 0.6 V and so contribute to the apparent activation barrier. Increasing the overpotential makes these oxidations more favorable so that the rate of O_2 release increases relative to water addition. This shifts the Sabatier maximum, the point at which the two reactions have the same degree of rate control, to a site with a higher basicity which favors water addition. In most of the low-potential regime, both sites are to the right of the Sabatier maximum so that increasing basicity decreases the rate; therefore the less basic (001) site is most active. In most of the medium potential regime, both sites are to the left of the Sabatier maximum so that increasing basicity increases the rate, therefore the more basic (311) site is most active.

Medium−High Potential Regime Transition; Relation to Oxidation Potential. At an overpotential of 0.77 V, the system transitions from the medium potential regime where the (311) dual-Co site is most active to the high potential regime where the (110) single-Co site is most active. As we will see, this transition is associated with a change in the resting oxidation state of the (110) site from Co(IV) to Co(V) and is thus related to the oxidation potential of the site.

The difficulty of sufficiently oxidizing the single-Co site on the (110) surface is the main reason for the higher TOF of the dual-Co sites on the (311) and (001) surfaces at the lower overpotentials. This results in a low fraction of oxidized (reactive) single-Co sites compared to oxidized dual-Co sites (which are nearly all oxidized at overpotentials above 0.5 eV). The energy to oxidize a single-Co site is the sum of the energy to deprotonate an η-OH, and the energy to remove an electron from the Co(IV) it is coordinating, forming the active Co(V)═O species. Both of these energies are high due to the unfavorable +V oxidation state required for the Co and the low acidity of the η-OH, leading to a low concentration of oxidized single-Co sites.

The energy to oxidize the dual-Co site is much lower as it involves deprotonation of a more acidic η-H_2O ligand and oxidation of a Co(III) to Co(IV). This is due to the fact that the two holes required to oxidize the incoming water are located on the two different Co(IV) centers of the dual-Co site, while the two holes are on the same Co(V) center in the single-Co site. Similar reasoning applies to the deprotonation that occurs during the oxidation; on the dual-Co site the protons are removed from two different oxygen atoms, while on the single-Co site they both come from the same oxygen atom.

At higher overpotentials, a greater fraction of the single-Co sites become oxidized. When the applied potential rises above the oxidation potential of this site, nearly all of them (as well as the dual-Co sites) are in the oxidized state, and the TOF is determined by the relative rate constant of O−O bond formation from the oxidized state. Since the activation barrier for O−O bond formation is lower on the single-Co site than on the dual-Co site, the single-Co site has a higher TOF at overpotentials where both sites exist primarily in the oxidized state. Whereas the single-Co site is more difficult to oxidize than the dual-Co site, once it is oxidized it is intrinsically more reactive for water addition, as has been explained in the section describing the quantum chemistry of the O−O bond formation step.

Relation to Oxidation Potential. The difference in the water addition barriers on the (311) dual-Co site and the (110) single-Co site is mainly due to differences in the electrophilicity of the oxo on the two sites. The basicity is similar for the two sites because both involve deprotonation of the water by an η-OH and therefore does not play a role. The terminal oxo on the single-Co site is more electrophilic than the bridging oxo on the dual-Co site which leads to a lower activation barrier. The electrophilicity is related to the energies and locations of the holes on the two species, with a higher energy hole that is more localized on the oxygen leading to a higher electrophilicity. The terminal oxo on the single-Co site is more electrophilic because having both holes on the same Co(V) cation is less favorable than having them on separate Co(IV) cations. As a result, the holes on the Co(V) are higher in energy and more readily localize on the oxygen atom to accept electrons donated from the attacking water.

The electrophilicity of the oxo is related to the oxidation potential of the active site via the hole energy. A site with high energy holes has a higher oxidation potential but is more electrophilic and reactive for water addition once it is in the oxidized state. This suggests that an additional Sabatier relationship exists involving the oxidation potential as a descriptor, shown in Scheme 3. When the oxidation potential of a certain site is below the applied potential (below the Sabatier maximum), most of the sites will be in the oxidized state, and an increase in oxidation potential has little effect on this fraction. Instead, the increase in oxidation potential is correlated with an increase in electrophilicity of the oxo and a decrease in intrinsic barrier leading to an increase in TOF. Once the oxidation potential is higher than the applied potential (above the Sabatier maximum), a further increase

DOI: 10.1021/jacs.5b07779
J. Am. Chem. Soc. 2015, 137, 14660−14672

will result in a decrease in the fraction of sites in the oxidized state and a decrease in the TOF. Thus, like the Sabatier curve based on Brønsted basicity discussed in the last section, this Sabatier curve is also not fixed but is dependent on the applied potential with a maximum existing at the point where the oxidation potential is equal to the applied potential.

Differences between Single-Co Sites on the (110) and (001) Surfaces. A final point to address is the higher TOF for water addition to a single-Co site on the (110) surface compared to a single-Co site on the (001) surface. This is due to the lower overpotential needed to oxidize the (110) site to the active state for water addition (0.80 vs 1.04 V) which is related to the coordination of the Co cation as shown in Figure 4. On the (001) site, this Co is coordinated to five surface

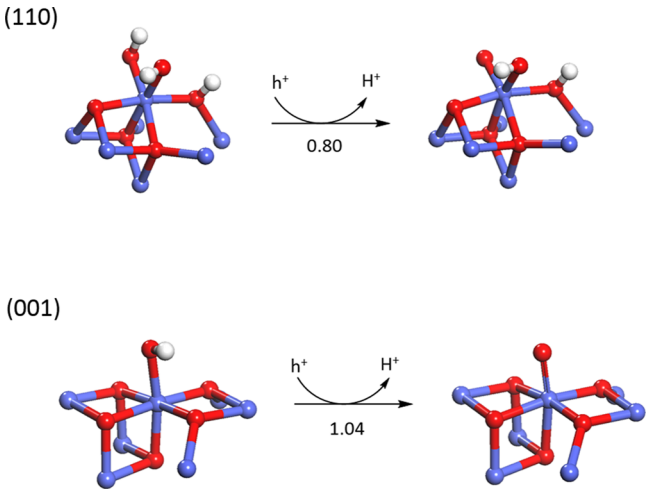

Figure 4. Comparison of the structures and energetics (eV at η = 0) for the oxidation of the single-Co site on the (110) and (001) surfaces prior to water addition. The lower oxidation potential of the (110) site is due to the stabilization of the Co(V) in the oxidized state by the basic η-OH.

oxygens and an η-oxo, while on the (110) surface, this Co is coordinated to an η-OH, four surface oxygens, and an η-oxo. The η-OH on the (110) surface is more basic than the surface oxygens and therefore better stabilizes the unoccupied 3d t_{2g} orbitals on the Co(V) leading to a lower oxidation potential.

Comparison with the Thermodynamic Approach. We would finally like to compare our results, as well as our computational approach, to the commonly used thermodynamic approach which does not consider reaction barriers.[33] According to this approach, the best OER catalyst is the one with the lowest-energy potential determining step. The potential determining step is defined as the electrochemical step with the highest free energy, and this determines the minimum overpotential at which all steps are downhill in free energy, which is called the thermodynamic overpotential. While this approach provides a very efficient and useful method to screen many different materials for potential OER activity, it does not always predict the correct mechanism due to the exclusion of reaction barriers, as has been already pointed out by Van Voorhis and co-workers.[34] This is especially true when it is considered that the site and mechanism can change with overpotential, something that a purely thermodynamic approach cannot account for.

The method used for the thermodynamic analysis, along with the results, are given in the Supporting Information. It should be noted that we use the catalytic cycles depicted in Scheme 1 (and in the Supporting Information for the active sites on the (001) surface) instead of the four-step cycle developed by Rossmeisl and co-workers.[30,31] This analysis gives similar thermodynamic overpotentials for the dual-Co sites on the (311) and (001) surfaces (0.60 V for (311) and 0.66 V for (001)). The slightly lower thermodynamic overpotential for the (311) site would indicate that it is active at a lower overpotential than the (001) site, in contrast to the kinetic results which indicate that the (001) site is more active at low overpotentials. The potential determining step predicted for the (001) site is water addition coupled with oxidation of the resulting hydroperoxo to a superoxo. On the (311) site, the potential determining step is oxidation of a Co(III) in the active site to Co(IV) prior to O_2 release. This does seem to correctly indicate that O_2 release is faster on the (001) site and water addition is faster on the (311) site. It does not, however, have any significance in determining the rate-limiting step since this is seen to change with overpotential, something that the thermodynamic model cannot account for.

Both of these failures of the thermodynamic approach for this system are due to the assumption implicit in this analysis that the barriers of all of the elementary reaction steps are small.[34] Based on the barriers we have calculated, it appears that this is not the case for water addition and O_2 release. The thermodynamic analysis works better for the single-Co sites, predicting thermodynamic overpotentials of 0.83 and 1.04 V for the (110) and (001) surfaces, respectively. This is consistent with our kinetic results which indicate that the (110) site has a higher TOF than the (001) single-Co site and that both of these sites become active at higher overpotentials than the dual-Co sites. Also, the thermodynamics correctly show that formation of the Co(V)=O is a difficult step. However, the thermodynamics do not show that the TOF of the (110) single-Co site overtakes the (311) dual-Co site at high overpotentials since this is entirely due to the lower intrinsic activation barrier of the (110) site.

There are also differences between the thermodynamics we calculate and those calculated in a recent study of the OER on the (001) surface.[36] This study finds that in the resting state of the catalyst at the thermodynamic overpotential of 0.76 V, the terminal sites on the surface are covered by 3/4 ML of oxo species and 1/4 ML of hydroperoxo. We find that terminal oxo species do not form on this surface until the overpotential is >1.04 V. This difference is likely due to the different values of the effective electron repulsion integral used for the Co 3d electrons (U) in the GGA+U method. They use a much lower value of 3.52 eV, compared to our value of 5.02 eV. This leads to an increase in the oxidation potentials as shown in the Supporting Information and in other studies.[37,51] As discussed further in the Supporting Information, the value depends on a compromise since it does not reproduce the reaction free energies from higher level calculations for all steps of a similar catalytic cycle on a model complex containing a single Co ion. However, the overpotential predicted in ref 36 is significantly higher than overpotentials measured experimentally of around 0.35 V.[12,13] These lower oxidation potentials also lead to a thermodynamic overpotential (0.76 V) that is significantly lower than the one we calculate (1.04 V) for the (001) single-Co site. However, the dual-Co site, which we find to have a significantly lower thermodynamic overpotential of 0.66 V, was not considered in this study. In summary, the different value for U and neglect of the dual-Co site cause the thermodynamic

DOI: 10.1021/jacs.5b07779
J. Am. Chem. Soc. 2015, 137, 14660−14672

results for the OER on the (001) surface in this study to be very different from those in the current study.

We do note that there is another computational study of the OER on the (110) surface that uses a larger value of U (5.9 eV) but gets a lower thermodynamic overpotential (0.57 V) than ours (0.83 V).[52] We suggest that this is due to the fact that the study does not consider resting states with different oxidation states of the Co cations. In the single resting state considered, there is one Co(III) and one Co(IV) in the surface layer (based on the stoichiometry of the slab). In our resting state, at the thermodynamic overpotential, all of the surface and half of the subsurface octahedrally coordinated Co cations are in the Co(IV) state.

Identification of the Experimentally Observed Active Site. The dual-Co site on the stepped (311) surface, which is the most active site at overpotentials between 0.46 and 0.77 V among those we have examined, appears to correspond to the "fast site" proposed by Frei and co-workers.[25] In agreement with the structure of the site that they propose, the (311) dual-Co site is also composed of two adjacent cobalt centers. We find, however, that the proposed mechanism involving nucleophilic attack of water on a terminal oxo is not favorable at the experimental overpotential, but instead a water attack on a bridging oxo occurs. This mechanism is not in disagreement with any of the experimental observations, however. There are, in fact, four key experimental results from the above cited work that support our identification of the (311) bridge site as the active site:

- It is observed experimentally that <1% of the exposed Co sites have high activity. This indicates that the active site must be a defect site such as the step site on the (311) surface rather than the energetically favorable (001) termination.
- A superoxo intermediate is observed in the experiments. This implies that O_2 release is at least competitive with water addition which we find to be the case only on dual-Co sites and not on single-Co sites. Also, it is observed that for a 300 ms pulse of the laser that drives O_2 evolution, only 64% of the expected O_2 yield is observed when compared to a laser pulse of 20 s. This suggests that there is an induction period of about 100 ms after initiation of the laser pulse during which time the superoxo intermediate is being built up. After termination of the laser pulse, however, the existing superoxo intermediate does not react further to form O_2. The only kinetic scenario where this could happen is if the rate constant for superoxo elimination via O_2 release is similar to the rate constant for its formation via water addition. We find this to be the case for the (311) bridge site where the apparent barriers for water addition and O_2 release at an overpotential of 0.53 V (close to the experimental overpotential) are 0.82 and 0.77 eV, respectively.
- In experiments carried out in isotopically labeled water ($H_2{}^{18}O$) with unlabeled Co_3O_4, the initial superoxo intermediate detected is singly labeled. This rules out water addition to an η-oxo on a single-Co site which should rapidly undergo oxygen exchange with the solvent giving a doubly labeled superoxo since the oxygen is contained in a labile η-H_2O or η-OH ligand. The oxygen in a μ^3-O or μ^3-OH is much more strongly bound and can only exchange with the solvent by O_2 evolution.
- The TOF of the (311) bridging site at an overpotential of 0.53 V is only 1.5 orders of magnitude lower than the experimentally measured TOF. This corresponds to a difference in activation energy of about 0.1 eV so our results are in good agreement considering the approximations made in our calculations (mainly the accuracy of DFT and the lack of the solvent and electric field). This is especially apparent when one compares to our calculated TOF on the (001) bridge site at the experimental overpotential which is nearly 5 orders of magnitude lower than the experimental value and even more so for our calculated TOF on the (110) terminal site which is nearly 7 orders of magnitude lower.

Nocera and co-workers[27] also suggest that the active site could be a μ-oxo in their study on an amorphous cobalt oxide/phosphate OER catalyst. Like Frei and co-workers, they also observe singly labeled and unlabeled O_2 in the product but not fully labeled O_2. They suggest that the oxygens in terminal ligands should exchange rapidly with the solvent so that the singly labeled O_2 may be produced from a bridging oxo. They do, however, note that it is possible that the reaction forming the singly labeled O_2 may not be the one responsible for the majority of the O_2 evolution.

Our results for O_2 evolution on the (110) terminal site are in good agreement with the theoretical study of Siegbahn and co-workers[38] on a molecular OER catalyst with a cubane-like Co_4O_4 core. They also find that the rate-limiting step is O−O bond formation by nucleophilic attack of water on a singlet η-oxo bound to a Co cation in a formal Co(V) oxidation state. At the overpotential they base their results on (0.47 V), the overall activation barrier they calculate (1.37 eV) is similar to ours (1.20 eV). Even the intrinsic barrier they get starting from the singlet terminal oxo (0.51 eV) is similar to ours (0.33 eV). This agreement is not surprising considering that the local geometries of active sites that we have studied on these surfaces are also based on the Co_4O_4 cubane structure. It is worth mentioning that we get this agreement despite the fact that we use different electronic structure methods (we use GGA+U, they use a hybrid GGA) and that they additionally use a continuum solvent model, while we do not take account of the solvent. Due to the size of the catalyst they model, however, they do not find a bridging oxo site with an activity approaching ours on the (311) surface. They do find a μ^2-O site on a Co_3O_3 cluster. This, however, has a significantly higher overall activation barrier (1.18 eV) compared to the dual-Co sites we examine on Co_3O_4. It is likely due to the fact that the μ^3-OH we find on the (311) surface is much more acidic than the μ^2-OH on their cluster; consequently, the overpotential at which the oxidation in the step preceding water addition becomes favorable is 0.82 V, significantly higher than our value of 0.51 V on the (311) dual-Co site.

There are two theoretical studies which conclude that O−O bond formation on the Co_4O_4 catalyst occurs by the direct radical coupling of two adjacent η-oxos, both bound to different Co(IV) cations.[48,53] For all of the surfaces we have studied, we were unable to find a stable Co(IV)−O^- species; these species required a significant amount of energy to transfer a proton from a Co(IV)−OH to another site on the surface. This could be due to the lack of a solvent in our calculations, while the cited studies included explicit water molecules. This would of course stabilize the negatively charged oxo. Even considering this, a Co(IV) oxo has never been observed previously; it lies to

DOI: 10.1021/jacs.5b07779
J. Am. Chem. Soc. 2015, 137, 14660−14672

the right of the "oxo wall" between Fe(IV) and Co(IV) due to the placement of an electron in a high energy π^* orbital.[54] Co(V) has one less electron and is isoelectric to Fe(IV), thus a Co(V)=O is possible, while a Co(IV)=O is likely not.

The other evidence against direct radical oxo coupling comes from the isotopic studies of Frei and co-workers mentioned earlier.[25] The initial formation of a singly labeled superoxo intermediate indicates that one of the oxygen atoms comes from a bridging site since oxygens in terminal sites would likely be exchanged quickly with the solvent prior to initiation of O_2 evolution. In the radical coupling mechanism, the superoxo is formed from two terminal oxos and would be expected to form only a fully labeled superoxo intermediate. Even if exchange of terminal ligands is not fast, the superoxo and O_2 produced initially by the radical coupling mechanism would then both contain only unlabeled oxygen, neither of which are detected.

CONCLUSIONS

We have studied the OER on three different surface terminations of Co_3O_4. It is found that this reaction can occur on two different types of active site: a single-Co site in which O−O bond formation occurs by nucleophilic attack of water on an η-oxo coordinated to a single Co(V) and a dual-Co site in which it occurs by attack of water on a bridging μ^3-oxo coordinated to two Co(IV) and a Co(II). Using activation barriers calculated for the two nonelectrochemical steps in the catalytic cycle−water nucleophilic addition and O_2 release−turnover frequencies (TOFs) were determined for the different sites as a function of overpotential. It was found that which site has the highest TOF is highly dependent on the overpotential. We identify three overpotential regimes corresponding to different dominant active sites: a low potential regime at overpotentials below 0.46 V where a dual-Co site on the (001) surface is most active, a medium potential regime at overpotentials between 0.46 and 0.77 V where a dual-Co site located at a step edge on the (311) surface is most active, and a high potential regime at overpotentials above 0.77 V where a single-Co site on the (110) surface is most active.

In the low potential regime, O_2 release, which involves deprotonation of the active site, is rate limiting so that the more acidic (001) site has the highest TOF. As the overpotential increases, O_2 release becomes faster relative to water addition so that the latter is rate limiting in the medium potential regime. Water addition involves protonation of the active site by the attacking water so that the more basic (311) site has the highest TOF in this regime. The higher basicity (and lower acidity) of the (311) site is due to reduced coordination of oxygen atoms on the step edge.

In both the low and medium potential regimes, the overpotential is not high enough to oxidize a significant fraction of the single-Co sites on the (110) surfaces since it has a much higher oxidation potential than the dual-Co sites. Consequently, the rate of water addition, which requires an oxidized site, is very low on the (110) site in these regimes. In the high potential regime, the overpotential is high enough to oxidize these sites. The higher oxidation potential is associated with a lower intrinsic activation barrier for water addition (which involves reduction of the active site) so that the (110) site has the highest TOF once the overpotential is high enough for it to be oxidized in the resting state. The oxidation potential is high for the (110) single-Co site because both holes needed to oxidize the water during the water addition step are placed on the same Co which is in the unfavorable Co(V) oxidation state. This also makes the η-oxo coordinated to the Co(V) very electrophilic in the water addition step, leading to the low intrinsic barrier. On the dual-Co sites, one hole is placed on each of the two Co sites so that they are in the more stable Co(IV) oxidation state. Consequently, the oxidation potential is lower but the oxidized site is less reactive for water addition than the oxidized single-Co site.

The two potential regime transitions (low−medium and medium−high) suggest the existence of two different overpotential-dependent Sabatier relations. The low−medium transition appears to be associated with a Sabatier relation based on the Brønsted basicity of oxygen anions in the active site, while the medium−high transition appears to be associated with a Sabatier relation based on the oxidation potential. The position of the Sabatier maximum in the two-dimensional descriptor space moves to higher basicity and oxidation potential as the overpotential increases.

Our results show that at an overpotential of 0.53 V, which is similar to the one present in experiments by Frei and co-workers studying the OER by suspended Co_3O_4 nanoclusters,[25] the dual-Co site on the (311) surface is most active, and the rate is controlled by both water addition and O_2 release. This finding is in agreement with the above-mentioned experimental results which observe a superoxo intermediate that appears to contain one oxygen from a μ-oxo and one from the solvent. This particular surface, which contains a step edge, also agrees with the structure sensitivity observed in these experiments where <1% of the exposed Co sites are found to be active; we find the energetically preferred (001) surface to be much less active at this overpotential. Furthermore, the TOF we calculate for this active site is within 1.5 orders of magnitude of the value measured in these experiments, while the other surfaces and mechanisms are found to have TOFs more than 5 orders of magnitude lower than the measured value. Together, these points strongly suggest that we have identified the highly active catalytic site observed for Co_3O_4.

The commonly used model based only on thermodynamics[30,31] predicts that the dual-Co sites are more active than the single-Co sites and that the most difficult step (on the dual-Co sites) is either O_2 release or water addition. While this is correct at certain overpotentials, this model does not account for the changes in active site and rate-limiting step that occur as the overpotential increases. Furthermore, it predicts the (311) dual-Co site to become active at a lower overpotential than the (001) dual-Co site, which is contrary to the more rigorous kinetic results of the current study.

ASSOCIATED CONTENT

Supporting Information

The Supporting Information is available free of charge on the ACS Publications website at DOI: 10.1021/jacs.5b07779.

Details of quantum chemical calculations; calculation of the on-site effective Coulomb integral (U); determining free energies of intermediates; location of transition states for water addition; derivation of kinetics of a two-step catalytic cycle; structures of the (001), (110), and (311) surfaces; details of oxidation of the surfaces; details of the water addition reaction; electronic transitions during water addition; details of the O_2 release reaction; catalytic cycles and thermodynamic analysis; details of electronic structure analysis; determining oxidation states of Co cations; method for extracting hole densities from

DOI: 10.1021/jacs.5b07779
J. Am. Chem. Soc. 2015, 137, 14660−14672

quantum chemical calculations; free energies of surface states; structures of surface states (PDF)
Tables and figures (PDF)

AUTHOR INFORMATION

Corresponding Authors

*R.A.v.Santen@tue.nl
*craig.plaisance@tum.de

Present Address

†Theoretical Chemistry and Catalysis Research Center, Technische Universität München, D-85747, Garching, Germany

Notes

The authors declare no competing financial interest.

ACKNOWLEDGMENTS

C.P. acknowledges partial support from NRSC-Catalysis and the Institute for Complex Molecular Systems at the Technical University of Eindhoven. We also acknowledge NWO for access to supercomputing facilities.

REFERENCES

(1) Ross, P. N. *J. Electrochem. Soc.* **1979**, *126* (1), 67.
(2) Ross, P. N. *J. Electrochem. Soc.* **1979**, *126* (1), 78.
(3) Koper, M. T. M. *Nanoscale* **2011**, *3* (5), 2054−2073.
(4) Gilliam, R. J.; Kirk, D. W.; Thorpe, S. J. *Electrocatalysis* **2012**, *3* (1), 68−74.
(5) Gilliam, R. J.; Kirk, D. W.; Thorpe, S. J. *Electrocatalysis* **2012**, *3* (2), 88−95.
(6) Gilliam, R. J.; Kirk, D. W.; Thorpe, S. J. *Electrocatalysis* **2011**, *2* (1), 1−19.
(7) Markovic, N. *Surf. Sci. Rep.* **2002**, *45* (4−6), 117−229.
(8) Maillard, F.; Pronkin, S.; Savinova, E. R. In *Fuel Cell Catalysis*; John Wiley & Sons, Inc.: Hoboken, NJ, 2008; pp 507−566.
(9) Solla-Gullón, J.; Vidal-Iglesias, F.; Herrero, E.; Feliu, J.; Aldaz, A. In *Polymer Electrolyte Fuel Cells*; Pan Stanford Publishing: Singapore, 2013; pp 93−151.
(10) Lebedeva, N. P.; Koper, M. T. M.; Feliu, J. M.; van Santen, R. A. *J. Phys. Chem. B* **2002**, *106* (50), 12938−12947.
(11) Chen, Q.-S.; Vidal-Iglesias, F. J.; Solla-Gullón, J.; Sun, S.-G.; Feliu, J. M. *Chem. Sci.* **2012**, *3* (1), 136.
(12) Nocera, D. G. *Acc. Chem. Res.* **2012**, *45* (5), 767−776.
(13) Zhang, M.; Frei, H. *Catal. Lett.* **2015**, *145* (1), 420−435.
(14) Lyons, M. E. G.; Brandon, M. P. *J. Electroanal. Chem.* **2010**, *641* (1−2), 119−130.
(15) Dinca, M.; Surendranath, Y.; Nocera, D. G. *Proc. Natl. Acad. Sci. U. S. A.* **2010**, *107* (23), 10337−10341.
(16) Suntivich, J.; May, K. J.; Gasteiger, H. a; Goodenough, J. B.; Shao-Horn, Y. *Science* **2011**, *334* (6061), 1383−1385.
(17) Walter, M. G.; Warren, E. L.; McKone, J. R.; Boettcher, S. W.; Mi, Q.; Santori, E. A.; Lewis, N. S. *Chem. Rev.* **2010**, *110* (11), 6446−6473.
(18) Marshall, A.; Børresen, B.; Hagen, G.; Tsypkin, M.; Tunold, R. *Energy* **2007**, *32* (4), 431−436.
(19) Van Santen, R. A.; Tranca, I.; Hensen, E. J. M. *Catal. Today* **2015**, *244*, 63.
(20) Woodruff, D. P. *Chem. Rev.* **2013**, *113* (6), 3863−3886.
(21) Haber, J. *Catal. Today* **2009**, *142* (3−4), 100−113.
(22) Haber, J. In *Handbook of Heterogeneous Catalysis*; Wiley-VCH Verlag GmbH & Co. KGaA: Weinheim, Germany, 2008.
(23) Volta, J. C.; Portefaix, J. L. *Appl. Catal.* **1985**, *18* (1), 1−32.
(24) Haber, J. In *Studies in Surface Science and Catalysis*; Elsevier: Amsterdam, **1989**; Vol. *48*, pp 447−467.
(25) Zhang, M.; de Respinis, M.; Frei, H. *Nat. Chem.* **2014**, *6* (4), 362−367.
(26) Jiao, F.; Frei, H. *Angew. Chem., Int. Ed.* **2009**, *48* (10), 1841−1844.
(27) Surendranath, Y.; Kanan, M. W.; Nocera, D. G. *J. Am. Chem. Soc.* **2010**, *132* (14), 16501−16509.
(28) Esswein, A. J.; Surendranath, Y.; Reece, S. Y.; Nocera, D. G. *Energy Environ. Sci.* **2011**, *4* (2), 499−504.
(29) Kanan, M. W.; Yano, J.; Surendranath, Y.; Dincă, M.; Yachandra, V. K.; Nocera, D. G. *J. Am. Chem. Soc.* **2010**, *132* (39), 13692−13701.
(30) Man, I. C.; Su, H.-Y.; Calle-Vallejo, F.; Hansen, H. a.; Martínez, J. I.; Inoglu, N. G.; Kitchin, J.; Jaramillo, T. F.; Nørskov, J. K.; Rossmeisl, J. *ChemCatChem* **2011**, *3* (7), 1159−1165.
(31) Rossmeisl, J.; Qu, Z.-W.; Zhu, H.; Kroes, G.-J.; Nørskov, J. K. *J. Electroanal. Chem.* **2007**, *607* (1−2), 83−89.
(32) Rossmeisl, J.; Dimitrievski, K.; Siegbahn, P.; Norskov, J. K. *J. Phys. Chem. C* **2007**, *111* (51), 18821−18823.
(33) Nørskov, J. K.; Rossmeisl, J.; Logadottir, A.; Lindqvist, L.; Kitchin, J. R.; Bligaard, T.; Jónsson, H. *J. Phys. Chem. B* **2004**, *108* (46), 17886−17892.
(34) Mavros, M. G.; Tsuchimochi, T.; Kowalczyk, T.; McIsaac, A.; Wang, L.-P.; Van Voorhis, T. *Inorg. Chem.* **2014**, *53* (13), 6386−6397.
(35) Quaino, P.; Juarez, F.; Santos, E.; Schmickler, W. *Beilstein J. Nanotechnol.* **2014**, *5*, 846−854.
(36) García-mota, M.; Bajdich, M.; Viswanathan, V.; Vojvodic, A.; Bell, A. T.; Nørskov, J. K. *J. Phys. Chem. C* **2012**, *116* (39), 21077−21082.
(37) Kwapien, K.; Piccinin, S.; Fabris, S. *J. Phys. Chem. Lett.* **2013**, *4* (24), 4223−4230.
(38) Li, X.; Siegbahn, P. E. M. *J. Am. Chem. Soc.* **2013**, *135* (37), 13804−13813.
(39) Cohen, a J.; Mori-Sanchez, P.; Yang, W. *Science (Washington, DC, U. S.)* **2008**, *321* (5890), 792−794.
(40) Anisimov, V. I.; Gunnarsson, O. *Phys. Rev. B: Condens. Matter Mater. Phys.* **1991**, *43* (10), 7570−7574.
(41) Liechtenstein, A. I.; Anisimov, V. I.; Zaanen, J. *Phys. Rev. B: Condens. Matter Mater. Phys.* **1995**, *52* (8), R5467−R5470.
(42) Anisimov, V. I.; Aryasetiawan, F.; Lichtenstein, A. I. *J. Phys.: Condens. Matter* **1997**, *9* (4), 767−808.
(43) Cococcioni, M.; de Gironcoli, S. *Phys. Rev. B: Condens. Matter Mater. Phys.* **2005**, *71* (3), 035105.
(44) Kulik, H. J.; Cococcioni, M.; Scherlis, D. A.; Marzari, N. *Phys. Rev. Lett.* **2006**, *97* (10), 103001.
(45) Roudgar, A.; Eikerling, M.; van Santen, R. *Phys. Chem. Chem. Phys.* **2010**, *12* (3), 614−620.
(46) Bajdich, M.; García-mota, M.; Vojvodic, A.; Nørskov, J. K.; Bell, A. T. *J. Am. Chem. Soc.* **2013**, *135* (36), 13521−13530.
(47) Betley, T. A.; Wu, Q.; Van Voorhis, T.; Nocera, D. G. *Inorg. Chem.* **2008**, *47* (6), 1849−1861.
(48) Wang, L.-P.; Van Voorhis, T. *J. Phys. Chem. Lett.* **2011**, *2* (17), 2200−2204.
(49) Mattioli, G.; Giannozzi, P.; Amore Bonapasta, A.; Guidoni, L. *J. Am. Chem. Soc.* **2013**, *135* (41), 15353−15363.
(50) McAlpin, J. G.; Surendranath, Y.; Dincă, M.; Stich, T. a; Stoian, S. a; Casey, W. H.; Nocera, D. G.; Britt, R. D. *J. Am. Chem. Soc.* **2010**, *132* (20), 6882−6883.
(51) Wang, L.; Maxisch, T.; Ceder, G. *Phys. Rev. B: Condens. Matter Mater. Phys.* **2006**, *73* (19), 195107.
(52) Chen, J.; Selloni, A. *J. Phys. Chem. Lett.* **2012**, *3* (19), 2808−2814.
(53) Mattioli, G.; Giannozzi, P.; Amore Bonapasta, A.; Guidoni, L. *J. Am. Chem. Soc.* **2013**, *135* (41), 15353−15363.
(54) Winkler, J. R.; Gray, H. B. *Structure and Bonding*; Springer: Berlin, Heidelberg, 2012; pp 17−28.

DOI: 10.1021/jacs.5b07779
J. Am. Chem. Soc. 2015, 137, 14660−14672